STRUCTURE AND HORIZONTAL DISTRIBUTION OF THERMAL UPDRAUGHTS IN A CLOUDLESS BOUNDARY LAYER IN SOUTH-BAVARIA

Thomas A. Hafner
Presented at the XIX OSTIV Congress, Rieti, Italy (1985)

Summary

A case study of the structure and horizontal distribution of thermal updraughts is presented for a fully convective, but cloudless boundary layer with moderate mean winds, using time series analysis techniques. Data of wind, temperature and moisture are gathered in 1 Hz time series with the highly instrumented research-aircraft P-3 (NOAA) on April 15, 1982, during the Alpine Experiment (ALPEX) on a traverse flight across Southern Bavaria in 1450 m MSL close below an isothermal layer.

Although there are two sections A1 and A2 with different horizontal updraught distributions, the results indicate, that the mean structure of the thermal updraughts is almost identical in both sections. The typical spacing between weak updraughts (1–2 m/s) is about 3 km and between strong updraughts (5 m/s) about 17 km.

Spectral analysis indicates a horizontal lenght-scale of the strongest updraught regions of about 1.3 km, whereas broader updraught systems and induced convective waves contribute most to the mean downward momentum flux at wavelenghts of about 4 km.

1. Introduction

Glider pilots and aerodynamicists frequently ask meteorologists about the structure and horizontal distribution of thermal updraughts. Their objective is to establish a more realistic weather model as basis for the theory of 'cruising-speed-optimization', in order to predict the speed range of a sailplane during cross-country flight. This information, together with the required circling minimum speed in thermals, is needed to optimize the design of new wing profiles.
The structure of isolated thermals is non-predictable and completely arbitrary due to the turbulent character of the motion. However, the physics of the evolution of thermals must be equally valid for all developments. Therefore, glider pilots often find thermals with similar scale characteristics, as reported by Leykauf (1983) and measured by McBean and McPherson (1976).
In order to get insight into the nature and distribution of thermal updraughts, and to find structural similarities, it is necessary to perform case studies with varying boundary conditions in accordance to the requirements of turbulence measurements. This paper is intended to contribute a further step towards the understanding of thermal convection and presents a case study of aircraft measurements in a fully developed convective boundary layer without cumulus clouds. The data for this study were measured on April 15, 1982, during the Special Observation Period (SOP) of the Alpine Experiment (ALPEX).

2. Synoptic situation and boundary layer development

The general weather situation on April 15 (see fig. 1) is characterized by a slowly filling low over the western Mediterranean and a high pressure area, extending from UK to western Russia. Its corresponding cloudless area covers western and central Europe (see fig. 2) and forms a southern boundary almost exactly with the northern rim of the Alps.
The boundary layer over South-Bavaria shows a strong diurnal variation (see fig. 3). Starting from 00 UTC, the rawinsonde data from Munich indicate an inertial oscillation (not shown here) and a broad maximum of the windspeed between 800 and 1500 m MSL, which is situated above a strong surface inversion and below the main inversion height in 2250 m MSL. At 06 UTC the entire boundary layer is more stable stratified due to warm air advection and surface layer cooling, and a remarkable low level jet with windspeeds up to 20 ms^{-1} has fully developed. At 12 UTC, which is close to the aircraft measurements, the boundary layer structure has completely changed: the surface temperature has increased due to radiation by 11°C. The stratification is superdiabatic in the lowest 100 m and then almost adiabatic in a well mixed layer up to 1600 m MSL, where a deep and subsiding isothermal layer stops the fully developed convection before condensation may lead to cumulus clouds. The wind blows constantly with height from East, whereas the windspeed increases from 5 ms^{-1} at the ground to 14 ms^{-1} at 1000 m MSL. The max-wind is found in 2350 m MSL with 16 ms^{-1} above the isothermal layer. The turbulent state of this boundary layer is described with the Gradient Richardson Number

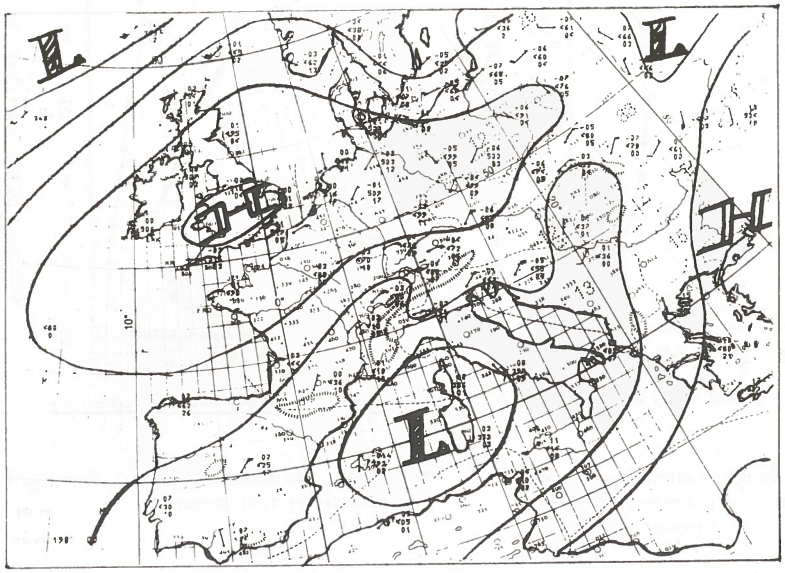

Figure 1: 850 hPa-weather chart for April 15, 1982, 00 UTC.

Figure 2: Satellite image of NOAA 7 VIS for April 15, 1982, 13.50 UTC.

which is computed from the rawinsonde Munich (12 UTC) and plotted versus height in fig. 4. Production of turbulent kinetic energy at $Ri < Ri_{crit} = 0.25$ is predicted inside of the convec tive layer with a distinct maximum in the unstable surface layer for $Ri < 0.$, whereas the turbulence is damped out inside and above the isothermal layer.

3. Flight mission, platform and data processing

On April 15, 1982, an ALPEX aircraft mission was conducted with the primary aim to investigate the Bora and second to search for the low level jet over South-Bavaria. After takeoff at 6.26 UTC in Geneva and the ferry flight to Yugoslavia, a very successful Bora mission was performed from 8.23 to 12.59 UTC (see fig. 5). After the night-time low-level jet over Bavaria had disappeared, the mission was continued as an ordinary ferry flight via Klagenfurt (K), Salzburg (S), Tölz (T), Ingolstadt (I) and Friedrichshafen (F) back to Geneva (touch down 15.20 UTC). The time period 13.44 - 14.30 UTC, denoted by P415, is selected for this case study. During this period the aircraft operated in the fair-weather zone north of the Alps and maintained flight level 45 (= 860 hPa or 1380 m MSL) inside the convective layer. Inflight observations confirm a vertical distance of about 200 m to the isothermal layer above, and report a persistent, moderate turbulence and a regular up and down motion of the aircraft due to thermal convection. In accordance to fig. 5 & 6 and table 1, the time period P415 is divided into the subperiods A1 between Tölz and Ingolstadt and the subperiod A2 between Ingolstadt and Friedrichshafen.

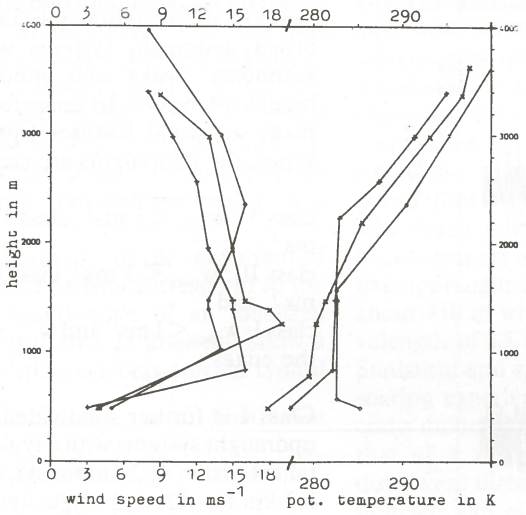

Figure 3: Rawinsonde data of Munich from April 15, 1982 (+ 00 UTC, x 06 UTC, 12 UTC).

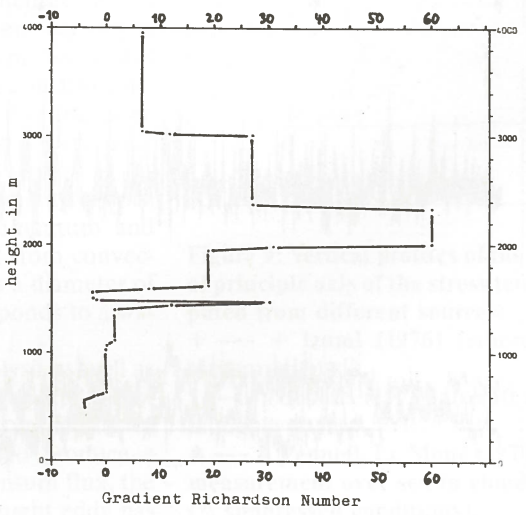

Figure 4: Gradient Richardson Number Profile of Munich from April 15, 1982.

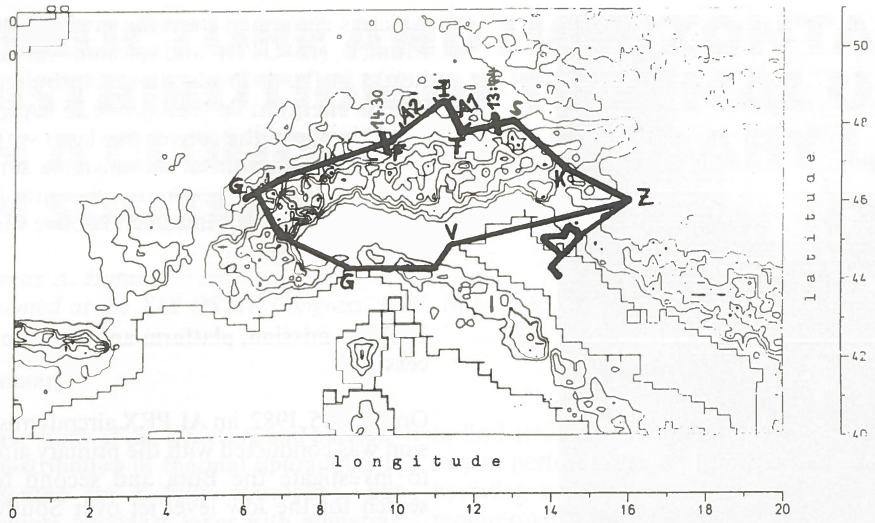

Figure 5: Flight track of P-3 of April 15, 1982.

Table 1: Flight sections and mean winds

Time		P415	A1	A2	RS Munich
From:	(UTC)	13:44:18	13:52:30	14:09:10	12
	sec	0	500	1500	
To:	(UTC)	14:29:57	14:05:49	14:22:29	
	sec	2739	1300	2300	
nb. of records		2740	800	800	
$\overline{U}$ in ms^{-1}		-10.8	-10.6	-13.0	
$\overline{V}$ in ms^{-1}		- 2.4	- 1.5	- 2.6	0.0

($\overline{U}$, $\overline{V}$ – mean wind in geographical coordinates).

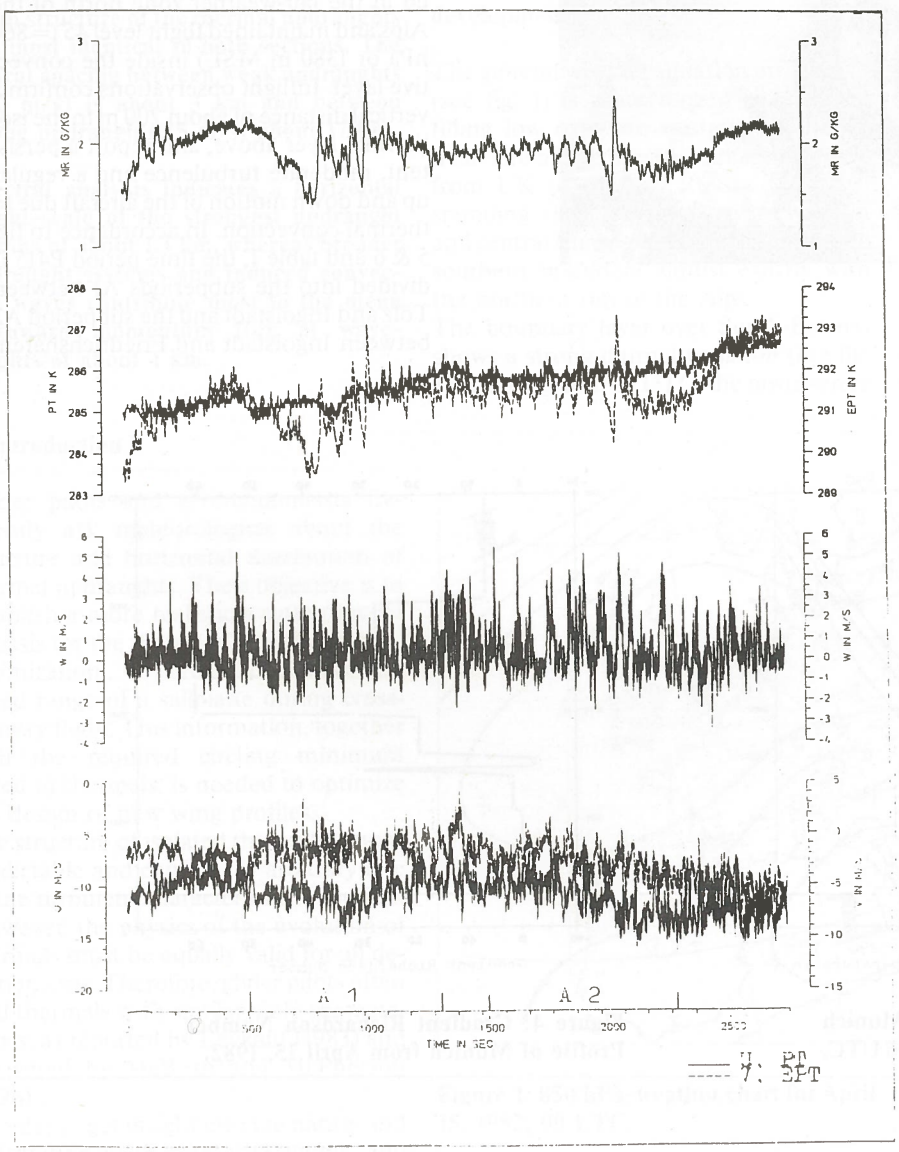

In addition, table 1 shows the good agreement of the measured easterly wind from the rawinsonde data and the aircraft data. The instrument platform is the four-engine turboprop aircraft Lockheed WP-3D (P3), which is owned and operated by the National Oceanic and Atmospheric Administration (NOAA) of the United States Department of Commerce.
Its instrumentation includes a wide range of meteorological, cloud physics and radiation sensors of high accuracy. Most of the measured parameters are on-line processed at a sampling rate of 1 Hz; time series of various parameters are already available during the flight on screen and as hardcopy. After landing the entire dataset gets reprocessed and quality proofed (for details see WMO, 1982).

4. Results

The time series of the measured meteorological parameters (before trend elimination and coordinate rotation) are presented in fig. 6 over the entire section P415. Two different types of convection become obvious in the subsections A1 and A2, expecially from the vertical velocity w.

Figure 6: Time series of measured parameters (u, v, w-windcomponents, PT, EPT-potential and equiv. pot. temperatures, MR-mixing ratio).

The w-pattern in A1 in very regular, high frequent and with low amplitudes ranging from +3.3 ms^{-1} to -2.4 ms^{-1}. In A2 a smaller number of larger and stronger updraughts is found with more irregular spacing and maxima of w between +5.5 ms^{-1} and -3.5 ms^{-1}.
The horizontal arrangement and the structural variability of single updraughts is shown in the high resolution time series of w from section A2 in fig. 7. Single slim peaks of strong updraughts alternate with broad updraught systems with several secondary peaks and moderate updraught intensities. In order to extract the main structural features from the time series, the updraughts are classified into:

class V: $w_{max} < 5$ ms^{-1}, class IV: $w_{max} < 4$ ms^{-1},
class III: $w_{max} < 3$ ms^{-1}, class II: $w_{max} < 2$ ms^{-1}, and
class I: $w_{max} < 1$ ms^{-1} and $w_{min} < 0{,}5$ ms^{-1} at the edges.

Class I is further subdivided into broad updraught systems with a typical horizontal extension of 2 km for A1, respectively 3.3 km for A2, and single updraught elements with a typical width of 800 m for A1 and 900 m for A2. According to this grouping, fig. 8 presents a histogram of the updraught class distribution on the left side, and the mean horizontal spacing between neighbouring updraughts of the

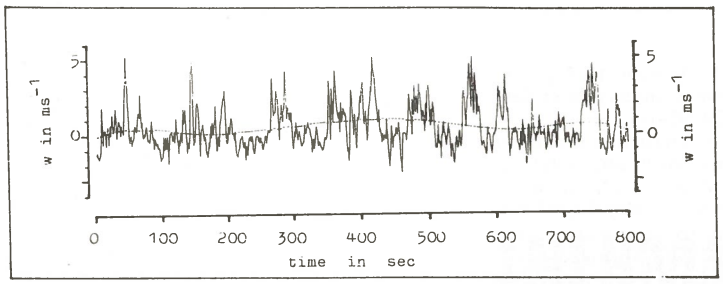

Figure 7: Time series of spline-detrended vertical wind component w dashed line is the spline function).

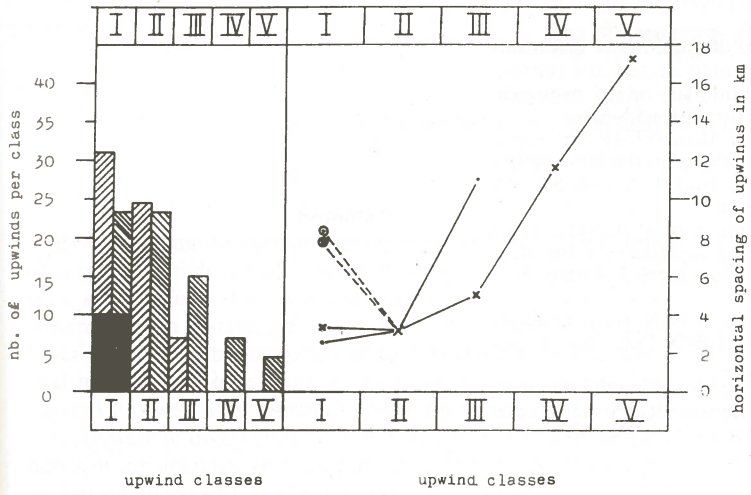

Figure 8: Left side: histogram of classified updraughts ([] A1, [] A2, [] broad updraughts).

same class on the right side. Broad updraught system appear equally in number in both sections A1 and A2, and they are similarly separated by a distance of about 8 km. Single updraught peaks of class I and II with a typical spacing of 3 km are most frequent. With increasing updraught intensity (class III to V), the number of updraught decreases dramatically, and the horizontal spacing increases in section A1 to about 10 km for updraughts of class III, and almost linearly in section A2 from class III with 5 km up to about 17 km in class V.

In order to describe the structure of idealized mean updraughts, spectral analysis and principle axis transformation was performed.

The wavelengths λ_m of the maximum of power spectral density correspond to the horizontal length-scale of an idealized upwind eddy. Table 2a does not show a significant difference between the typical extensions of the updraught systems in section A1 and A2. The wavelengths of the eddies with maximum energy content (underlined in table 2a and 2b) are situated between 1.28 km and 1.59 km for the u- and w-component and agree well with the estimates of the strong type of updraughts from the histogram in fig. 8. The structural elements with the most efficient transport of momentum (u'w') and heat (w'O'), however, occure at wavelenghts of about 4 km. Since this wavelength is not favoured in the v'w'-cospectra, it is presumed that the main momentum and heat flux is carried by convective gravity waves which are induced from the broad updraught systems. The lower portion of momentum and heat transport is managed from convective updraught eddies with a diameter of about 750 m which corresponds to a wavelength of 1.5 km.

Statistical and spectral analysis as well as soaring experience favour an updraught eddy model with a structure similar to that of a rotating tube. To produce a downward directed momentum flux, the principle axis of this updraught eddy has to be tilted from the vertical at an angel $-\alpha$ into the direction of the mean horizontal wind.

The values of the normalized Root Mean Square (RMS) wind components, the turbulent kinetic energy E, the computed tilt angles $-\alpha$ and the heat fluxes are listed in table 3.

Table 2a: Wavelength λ_m in km from power spectra.

	u-spectrum	v-spectrum	w-spectrum
A1	1.28	2.0 0.5	1.32
A2	1.33	1.82 1.33	4.54 1.59 0.71

Table 2b: Wavelength λ_m in km from cospectra.

	uw-cospectrum	vw-cosprectrum	w0-cospectrum
A1	4.00 1.61 1.28 1.03	2.17	3.85 2.08 1.67
A2	4.35 1.50	10.87 1.43 0.77	4.35 1.68

Table 3: Normalized RMS of wind components, turbulent kinetic energy, tilt angles and heat fluxes.

	P415	A1	A2
RMS_u/u_{*1}	2.06	2.35	1.93
RMS_v/u_{*1}	2.00	2.63	1.61
RMS_w/u_{*1}	1.84	2.14	1.85
$3/2\ E/u_{*1}^2$	3.88	5.67	3.25
$-\alpha$ in degr	33.7	32.1	40.6
$H = pc_p w'o'$ in Wm^{-2}	55.3	44.2	88.4

The tilt angle, which varies between 32 degrees in A1 and 41 degrees in A2, is a very sensitive quantity with respect to the wind RMS variations (Hafner, 1981). Therefore, it is used to compare the results of this case study with previous measurements and numerical model results. In fig. 9 tilt angles, which are calculated from the statistics of several authors, are plotted against the dimensionless height x_3/z_i as lowest inversion height. Although, there exist only few measurements from the upper part of the Ekman-layer, the present results, denoted by A1

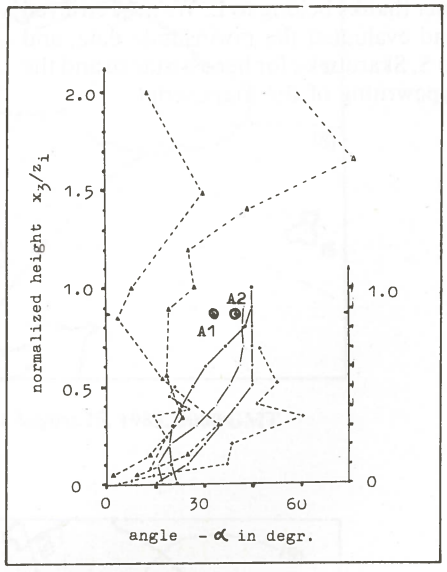

Figure 9: Vertical profiles of the tilt angle of principle axis of the stress tensor, computed from different sources:
+ --- + Izumi (1976) tethered ballon measurements
· --- · Nicholls (1978) aircraft measurements over sea
▲--- ▲ Pennell, Le Mone (1974) aircraft measurement over sea in cloudy regions (△ suppressed conditions).
·—· Deardorff (1972) 3-d boundary layer model
x—x Shir (1973) 3-d turbulence model
○—○ Wyngard (1975) second order closure model
0 values of the present case study.

and A2, are at least in good agreement with numerical results from boundary layer and turbulence models.

5. Conclusion

The present case study demonstrates, that important details about the structure and horizontal distribution of convective elements can be deduced by applying simple statistical methods to the time serial data of a ferry flight, which are usually treated as waste of a research flight mission. This information, however, has important practical value for glider pilots, aerodynamicists and boundary layer meteorologists.
It is therefore recommended that more of these so-called 'useless data' should be retrieved and evaluated towards a basic statistical approach of the problem, because convection is an arbitrary and turbulent type of motion. Nevertheless, it is also necessary to perform highly sophisticated boundary layer experiments with several simultanously operating powered gliders to study the physics of three-dimensional boundary layer convection.

Acknowledgement

The author is particularly grateful to the flight crew and the participating scientists of ALPEX – flight P415, especially to the mission scientist Prof. R. B. Smith. Further thanks belong to L. Weisel, retrieved and evaluated the rawinsonde data, and to S. Skaroupka for her assistance and the typewriting of the manuscript.

References

Deardorff, J.W. (1972): Numerical investigation of neutral and unstable planetary boundary layer, J. Atmos. Sci., 29, 91–115.
Hafner T.A. (1981): Turbulenzstrukturen in der atmosphärischen Grenzschicht abgeleitet aus den Varianzen der Windgeschwindigkeitskomponenten, Diplomarbeit Met. Inst. Univ. Karlsruhe, FRG.
Izumi, Y., J.S. Caughey (1976): Minnesota 1973 atmospheric boundary layer experiment data report, Environmental Res. Pap. No. 547, AFCRL-TR-76-0038.
Leykauf, H. (1983): Meteorological navigation of alpine long distance soaring flights. OSTIV Publication XVII.
Mc Bean, G.A., J.J. Mc Pherson (1976): Turbulence above Lake Ontario: Velocity and scalar statistics, Boundary-Layer Meteorol., 10, 181–197.
Nicholls, S. (1978): Measurements of turbulence by an instrumented aircraft in a convective atmospheric boundary layer over sea, Quart. J. R. Met. Soc., 104, 653–676.
Pennell, W.T., M.A. Le Mone (1974): An experimental study of turbulence in the fair-weather trade wind boundary layer, J. Atmos. Sci., 31, 1308–1323.
Shir, C.C. (1973): A preliminary numerical study of atmospheric turbulent flows in the idealized planetary boundary layer, J. Atmos. Sci., 30, 1327–1339.
WMO/ICSU (1982): ALPEX data management plan, GARP-ALPEX Publ. No. 4, Geneva.
Wyngaard, J.C. (1975): Modelling the planetary boundary layer – extension to the stable case, Boundary-Layer Meteorol., 9, 441–460.